DNS of Reacting Hypersonic Turbulent Boundary Layers

M. Pino Martín
V. Gregory Weirs
Debra Olejniczak
Graham V. Candler
Department of Aerospace Engineering and Mechanics
Army High Performance Computing Research Center
University of Minnesota, Minneapolis MN 55455

Abstract

A direct numerical simulation (DNS) approach is used to simulate boundary layers at supersonic speeds. The computational method is validated by comparison with experimental results of a Mach 0.3 turbulent boundary layer. Non-reacting supersonic turbulent boundary layer simulation parameters, such as the mean velocity, shear stress, structure parameter, and turbulent intensity, are found to be in agreement with experimental data. A Mach 4 turbulent boundary layer is simulated, which is represents a 26° wedge at a Mach number of 20 and 20 km altitude. In this case, the boundary layer temperature is high enough to induce chemical reactions. The endothermic chemical reaction that we simulate significantly reduces the temperature fluctuations in the boundary layer. The spanwise and wall-normal Reynolds stresses and the shear stress are increased. In addition, the pressure-dilatation increases by an order of magnitude.

Introduction

The boundary layers on proposed air-breathing hypersonic cruise vehicles will be hot, turbulent and chemically reacting. To design these hypersonic vehicles, we need a clear understanding of the physical processes that govern these flows; in the present paper, we perform DNS of hypersonic reacting turbulent boundary layers.

Thus far, our understanding of the interaction between turbulent motion and chemical reactions in hypersonic flows is somewhat limited. With the very high energies present in hypersonic flows, the temperature fluctuations will be very large. The reaction rate depends exponentially on temperature, and temperature fluctuations result in large increases in the reaction rates. Also, the chemical source term can either damp or amplify turbulent fluctuations; this effect has been seen experimentally by several researchers. Griffiths *et al.*[1] and Johnson *et al.*[2] have shown that under certain circumstances the flow downstream of a normal shock wave may become unstable due to exothermic recombination reactions. Recent linear stability analysis by Johnson *et al.*[3] have also shown that hypersonic boundary layers tend to be stabilized by endothermic reactions and destabilized by exothermic reactions.

Martín and Candler[4] use DNS to perform a fundamental study of isotropic turbulence interacting with finite-rate chemical reactions at conditions typical of a hypersonic boundary layer. They find that the turbulent motion is fed from the external energy provided by the exothermic reactions, while the reaction rate is increased by the turbulent temperature fluctuations. Martín and Candler[4] show that the feedback takes place through the pressure-strain term in the Reynolds stress equation. This feedback is negative for endothermic reactions. These findings are of great relevance to the physics of hypersonic turbulent boundary layers, however they need to be generalized for such flows and DNS must be used to do so since it is the most accurate tool.

Performing DNS of hypersonic boundary layers is not an easy task. The typical explicit time integration methods are very costly. However, new time integration methods make it possible to perform DNS of compressible boundary layers at reduced computational costs. Olejniczak and Candler[5] modify the Data Parallel Lower-Upper Relaxation DPLU method of Wright and Candler[6] for use in the DNS of compressible flows. The second-order accurate, implicit, time integration method DPLU reduces the computational cost by about a factor of three when the method is compared to a third order accurate Runge-Kutta method. Also, to capture the strong gradients that are present in hypersonic flows, an essentially non-oscillatory (ENO) scheme should be used. These schemes are generally expensive. Weirs and Candler[7] optimized a set of ENO schemes for use in compressible turbulent flows. Weirs *et al.*[8] combine the DPLU method with an optimized ENO scheme to perform DNS of hypersonic turbulent boundary layers. This method captures shock waves while maintaining high order accuracy and excellent dissipation and dispersion properties required to re-

solve the turbulent length scales. We use these new techniques to perform DNS of reacting, hypersonic, turbulent boundary layers.

The remainder of the paper is organized as follows. We first review the equations of motion of a reacting fluid. We discuss the numerical method and validate the computer implementation by comparing DNS of a Mach 0.3 turbulent boundary layer to experimental results. We describe the initialization process for non-reacting and reacting temporal boundary layers at supersonic Mach numbers. Finally, we discuss the results from a preliminary DNS of a reacting turbulent boundary layer.

Governing equations

Let us consider the equations that describe the conservation of mass, momentum, and energy in a reacting flow. For simplicity, we neglect the contribution of the internal energy modes. (For more details see Lee.[1]) The conservation equations can be written as

$$\begin{aligned}
&\frac{\partial \rho_s}{\partial t} + \frac{\partial}{\partial x_j}\Big(\rho_s u_j + \rho_s v_{sj}\Big) = w_s \\
&\frac{\partial \rho u_i}{\partial t} + \frac{\partial}{\partial x_j}\Big(\rho u_i u_j + p\delta_{ij} - \tau_{ij}\Big) = 0 \qquad (1)\\
&\frac{\partial E}{\partial t} + \frac{\partial}{\partial x_j}\Big((E+p)u_j - u_i\tau_{ij} + q_j + \sum_s \rho_s v_{sj} h_s\Big) = 0
\end{aligned}$$

where w_s represents the rate of production of species s due to chemical reactions; ρ_s is the density of species s; u_j is the mass-averaged velocity in the j direction; v_{sj} is the diffusion velocity of species s; p is the pressure; τ_{ij} is the shear stress tensor given by a linear stress-strain relationship; q_j is the conductive heat flux; h_s is the specific enthalpy of species s; and E is the total energy per unit volume given by

$$E = \sum_s \rho_s c_{vs} T + \tfrac{1}{2}\rho u_i u_i + \sum_s \rho_s h_s^\circ, \qquad (2)$$

where c_{vs} is the specific heat at constant volume of species s; and h_s° represents the heat of formation of species s.

To derive the expression for w_s, consider a reaction where species S1 reacts to form species S2

$$\mathrm{S1} + \mathrm{M} \rightleftharpoons \mathrm{S2} + \mathrm{M}, \qquad (3)$$

where M represents a collision partner, which is either S1 or S2 in this case. The source terms for S1 and S2 can be written using the law of mass action

$$\begin{aligned}
w_{\mathrm{S1}} = &- M_{\mathrm{S1}} k_f \frac{\rho_{\mathrm{S1}}}{M_{\mathrm{S1}}}\Big(\frac{\rho_{\mathrm{S1}}}{M_{\mathrm{S1}}} + \frac{\rho_{\mathrm{S2}}}{M_{\mathrm{S2}}}\Big) \\
&+ M_{\mathrm{S1}} k_b \frac{\rho_{\mathrm{S2}}}{M_{\mathrm{S2}}}\Big(\frac{\rho_{\mathrm{S1}}}{M_{\mathrm{S1}}} + \frac{\rho_{\mathrm{S2}}}{M_{\mathrm{S2}}}\Big),
\end{aligned} \qquad (4)$$

and $w_{\mathrm{S2}} = -w_{\mathrm{S1}}$. The forward and backward reaction rates are k_f and k_b respectively. These are written as

$$\begin{aligned}
k_f &= C_f\, T^\eta\, e^{-\theta/T}, \\
k_b &= \frac{k_f}{K_{eq}},
\end{aligned} \qquad (5)$$

where C, η, and θ are experimentally-determined constants, and K_{eq} is the known temperature-dependent equilibrium constant.[9]

For a two species mixture, the diffusion velocity can be accurately represented using Fick's law

$$\rho_s v_{sj} = -\rho D \frac{\partial c_s}{\partial x_j}, \qquad (6)$$

where $c_s = \rho_s/\rho$ is the mass fraction, and D is the diffusion coefficient given in terms of the Lewis number

$$Le = \frac{\rho D Pr}{\mu}, \qquad (7)$$

where Pr is the Prandtl number, μ is the viscosity, and Le is taken to be unity, so that the energy transport due to mass diffusion is equal to the energy transport due to thermal conduction.

Numerical method and code validation

We use a numerical method combining ENO scheme for the inviscid fluxes with an implicit time advancement technique. Derivatives required for the viscous terms are evaluated using 4th-order central differences. The ENO scheme was designed for low dissipation by Weirs and Candler[7] and provides shock-capturing, which is necessary at the Mach numbers considered in this paper. The time advancement technique is based on the DPLU relaxation method of Candler *et. al*,[10] and was extended to second-order accuracy by Olejniczak and Candler.[5] (We caution the reader that a time accuracy term is inadvertently left out of the relaxation loop derivation given in Olejniczak and Candler.[5]) The ENO scheme combined with the second-order DPLU time advancement has been successfully used for non-reacting boundary layer simulations by Weirs *et al.*[8] The algorithm is implemented on a distributed massively parallel supercomputer Cray T3E.

We validate the computer program by performing a DNS of a non-reacting turbulent boundary layer. We use periodic boundary conditions in the streamwise and spanwise directions. The density at the isothermal wall is given by the solution of the mass-conservation equations. We implement channel flow boundary conditions at the top boundary. The initial

field and computational grid of a $Re_\theta = 740$, $M = 0.3$, $T_w = T_\infty = 300$ K, $\rho_\infty = 1$ kg/m^3 turbulent boundary layer were provided by Piomelli.[11] The computational grid is equispaced in the periodic directions and exponentially stretched in the wall-normal direction. The size of the computational domain is $20\delta \times 5\delta \times 3\delta$ with $192 \times 128 \times 96$ grid points in the streamwise, spanwise and wall-normal directions respectively, where δ is the boundary layer thickness. The grid spacings correspond to $\Delta x^+ \approx 30$, and $\Delta y^+ \approx 10$ in the streamwise and spanwise directions. In the wall-normal direction the second grid point is at $z^+ = 0.1$.

Figure 1 plots the mean velocity profile for the above simulation. The square symbols show that the initial field is not stationary. The triangles illustrate the profile after the initial transient. At this time, the boundary layer has advanced one plate length, and $Re_\theta = 930$. The final velocity profile is in good agreement with the theoretical viscous sublayer and logarithmic region.

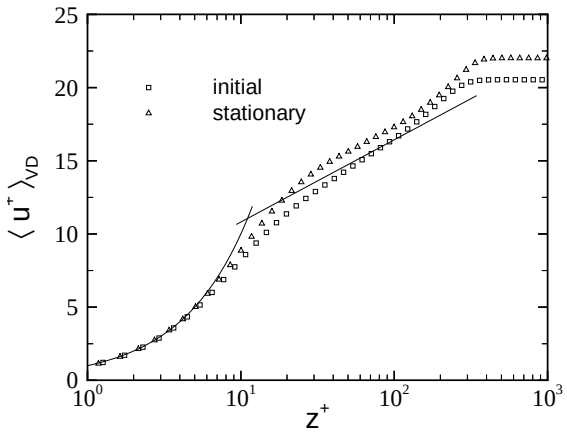

FIGURE 1. Mean streamwise velocity with Van Driest transformation for the boundary layer at $M = 0.3$. The solid lines represent $u^+ = z^+$ in the viscous sublayer, and $2.44 \log z^+ + 5.2$ in the logarithmic region.

Figure 2a plots the nondimensional shear stress, $\langle -u'w' \rangle / u_\tau^2$. Where u' and w' are the velocity fluctuations in the streamwise and normal directions and u_τ is the friction velocity. We observe that after the initial transient, there is a plateau in the region of maximum shear stress. The maximum value is 1.06. For $Re_\theta = 670$, experiments[12] predict a maximum value of about 0.95. Figure 2b plots the structure parameter, $\langle -u'w' \rangle / q^2$, across the boundary layer. Where q^2 is $\langle u_i' u_i' \rangle$. We find the structure parameter in [0.14:0.17] for $0.2 \leq z/\delta \leq 0.8$, after the initial transient. Experiments[13] predict a structure parameter in [0.14:0.16] for $0.1 \leq z/\delta \leq 0.8$. Figure 2c shows the distribution of the nondimensional longitudinal turbulent intensity, u'_{RMS}/u_τ. The maximum value occurs at $z^+ = 11$ for the initial field, which moves to the experimentally predicted location of $z^+ = 15$ after the initial transient. We also observe the development of a second maximum. After the initial transient time, the second maximum occurs at $z^+ \approx 255$ in the log-law-region of the mean profile, as observed experimentally. The agreement between the DNS and the experiments validates the implementation of the numerical method.

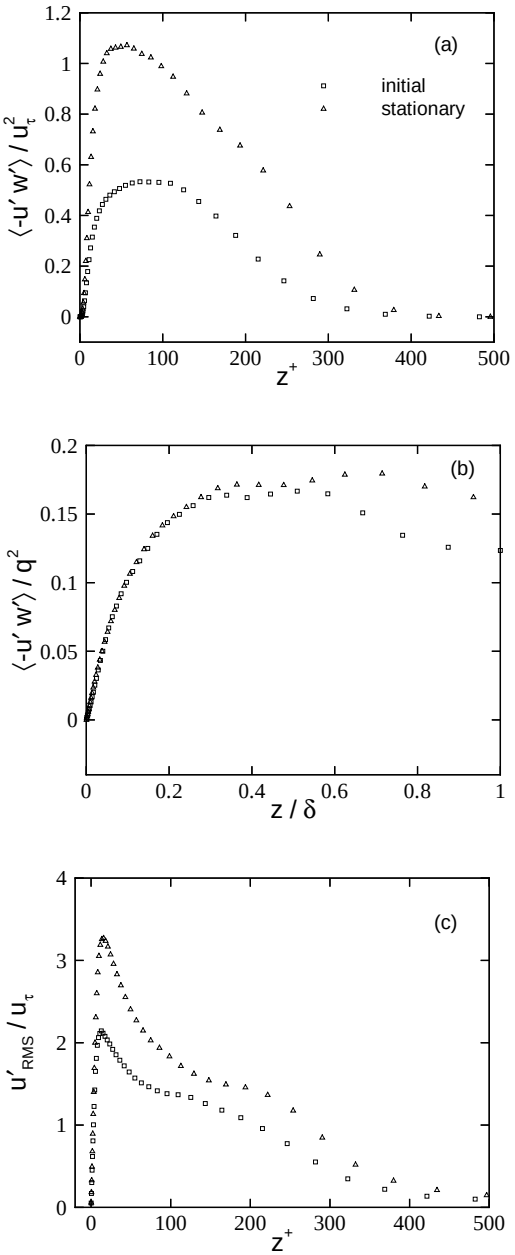

FIGURE 2. (a) Nondimensional shear stress, (b) structure parameter, and (c) nondimensional longitudinal turbulent intensity across the boundary layer at $M = 0.3$.

Non-reacting Results

We require simulations of hot, supersonic boundary layers. To initialize such fields, we use the results from a $k-\epsilon$ model to obtain the mean turbulent profiles and we use the fluctuating quantities from the Mach 0.3 turbulent field described in the previous section. In this section, we describe the procedure for the initialization of two turbulent fields at Mach 2 and 4.

We use the $k-\epsilon$ model by Jones and Launder[14] to compute the velocity, density, and temperature mean profiles and the inner parameters, u_τ and z_τ, at the desired Mach number, where $z_\tau = \frac{\mu_w}{\rho_w u_\tau}$. We normalize the Mach 0.3 fluctuating velocity field and computational domain by the ratio of the wall parameters at the high Mach number to that at 0.3. In this way, the fluctuating velocity is scaled proportionally to the Mach number. The grid resolution based on wall units remains unchanged after the transformation.

We interpolate the $k-\epsilon$ velocity, temperature and density mean profiles along the wall-normal direction. To match the Re_θ given by the $M = 0.3$ DNS with that given by the $k-\epsilon$ model, we use a mean density profile at $\rho_\infty = 0.5$ kg/m^3. We copy the mean profiles in the streamwise and spanwise directions to fill in the computational domain. Finally, we use the strong Reynolds analogy[15] to estimate the initial fluctuations in the thermodynamic variables.

We perform a DNS and monitor the two-point correlations, the energy spectra, and the mean velocity profiles to check the resolution and validity of the generated fields. Figure 3 plots the two-point correlations, $R_{\rho\rho}$, R_{uu}, R_{vv}, R_{ww}, R_{TT}, along the periodic directions for a $M = 2$ generated field at $z = 0.04\delta$ and $z = \delta$. The correlations are nearly zero in the middle of the domain. Thus, the computational domain is long enough to enclose a good statistical sample of the large structures in the field. When the same data analysis is done for the $M = 4$ field, we observe that the computational domain is not large enough.

To circumvent this problem, we double the domain size and the number of grid points in each periodic direction and reflect the fluctuating fields into the new grid portions. We also increase the number of points in the wall-normal direction from 96 to 128 grid points and fill it with free-stream conditions.

We perform a DNS and monitor the decay in the correlations during the transient time. Figure 4 illustrates the correlations for the $M = 4$ field after the flow has advanced 15% of the plate length. We observe that the correlations are negligible in the center of the domain except for those in the temperature fluctuations at $z = \delta$. We have continued the simulation until the flow advances 50% of the plate length. However, correlations do not decrease further. The length of the turbulent structures increases with the Mach number, thus we expect a higher correlation in the streamwise direction. However, we cannot explain the reason for the higher correlation in the spanwise direction. One could think that the higher coherence is due to acoustic disturbances present in the DNS. However, we find that the density-temperature interaction at $z = \delta$ is mostly of a non-acoustic nature. Figure 5 plots the joint probability density of density *vs.* temperature at $z = \delta$ for the $M = 4$ simulation. We observe that ρ' and T' are negatively correlated. The correlation between ρ' and T' would have to be positive to have a purely isentropic flow.

Figure 6 plots the 2-dimensional energy spectra. We observe that the turbulent cascade decays over 5 decades, showing that the field is well resolved.

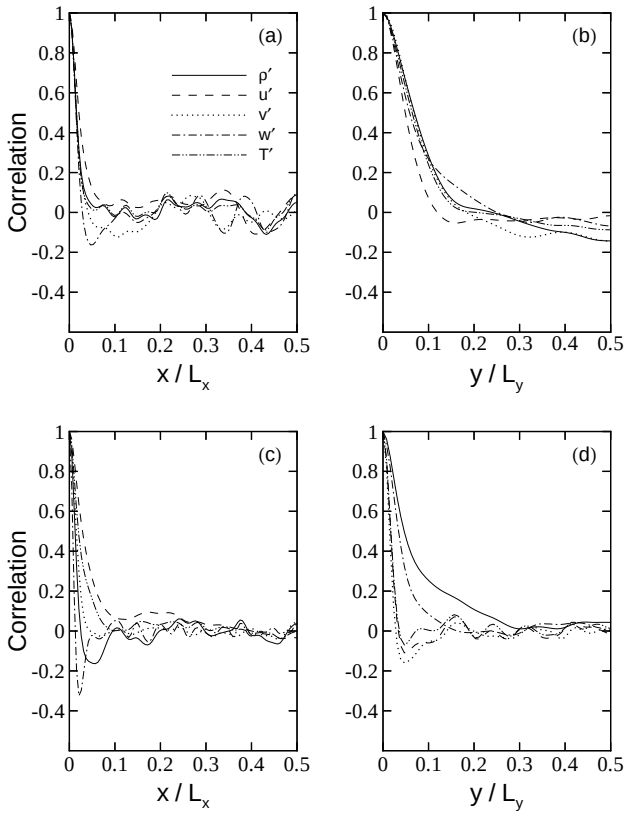

FIGURE 3. Two-point correlations at (a,b) $z = \delta$, and (c,d) $z = 0.04\delta$ at $M = 2$. Where Lx and Ly are the lengths in the streamwise and spanwise directions, respectively.

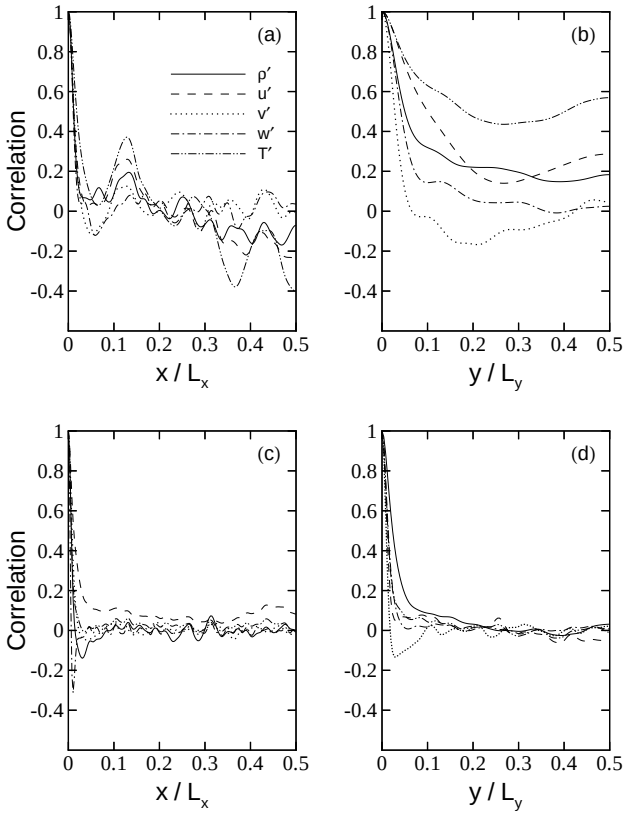

FIGURE 4. Two-point correlations at (a,b) $z = \delta$, and (c,d) $z = 0.04\delta$ at $M = 4$.

Figure 7 plots the mean velocity profiles for the three Mach numbers using the Van Driest transformation. Whereas the profiles for the Mach 0.3 and 2 simulations are in agreement with the theory, the Mach 4 case differs in the logarithmic region. However, this is not a consequence of the DNS. We have observed that the profiles given by the $k - \epsilon$ model consistently differ from the theory as the Mach number is increased, and the wall boundary condition is isothermal.

The size of the computational domain for the Mach 4, $\rho_\infty = 0.5\text{kg/m}^3$, and $T_w = T_\infty = 300\text{K}$ case is $20\delta \times 5\delta \times 17\delta$, with $384 \times 256 \times 128$ grid points in the streamwise, spanwise and wall-normal directions respectively. The grid spacings are $\Delta x^+ \approx 30$, $\Delta y^+ \approx 10$. In the wall-normal direction the second grid point is located at $z^+ = 0.1$. Since we continue the progressive stretching in the wall-normal direction for the added grid portion, the transformed domain is larger than necessary. Thus, an equally spaced grid could have been used to fill in the computational domain in the wall-normal direction from 96 grid points to 128. After the initial transient time, we find $Re_\theta = 1350$.

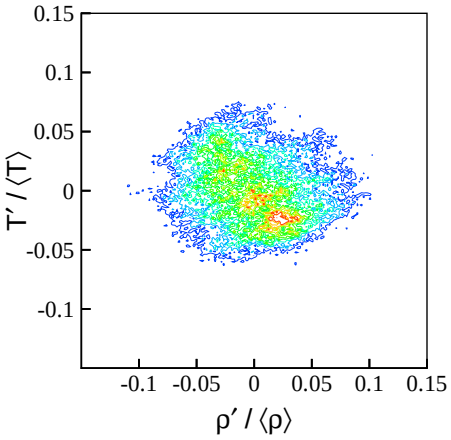

FIGURE 5. Joint-probability density of density *vs.* temperature at $z = \delta$ for the boundary layer at $M = 4$.

Figure 8 plots the longitudinal turbulent intensity for the $M = 4$ boundary layer as it appears in Daussauge and Gaviglio[16] (Fig. 4.) The DNS is in agreement with the data compilation except that we do not observe a second maximum. However, for compressible flow the second maximum is observed at very high Reynolds numbers and the maximum is not as pronounced as it is in incompressible flows. This may explain why at Re_θ=1350, we do not observe a second maximum. We use this $M = 4$ turbulent field to initialize the chemistry conditions.

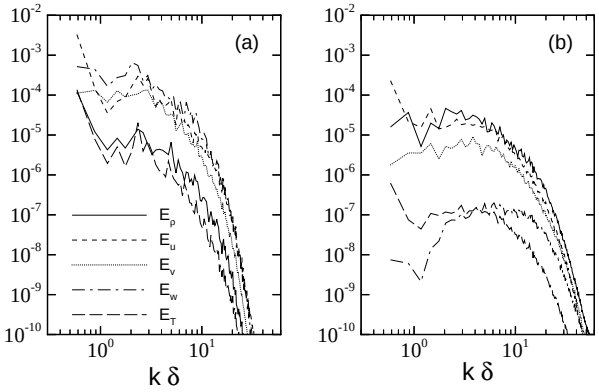

FIGURE 6. Two-dimensional energy spectra at (a) $z = \delta$, and (b) $z = 0.04\delta$ at $M = 4$.

Reacting Results

To initialize the reacting flow field, we multiply the temperature and the streamwise velocity component by 16.67 and 4.08, respectively, so that the edge temperature and Mach number are $T_\infty = 4980\text{K}$ and $M = 4$. We modify the expression for the viscosity to $\mu = \mu_\circ \left(\frac{T}{16.67 T_\circ}\right)^{0.72}$ so that the Reynolds number does not change after rescaling the temperature. How-

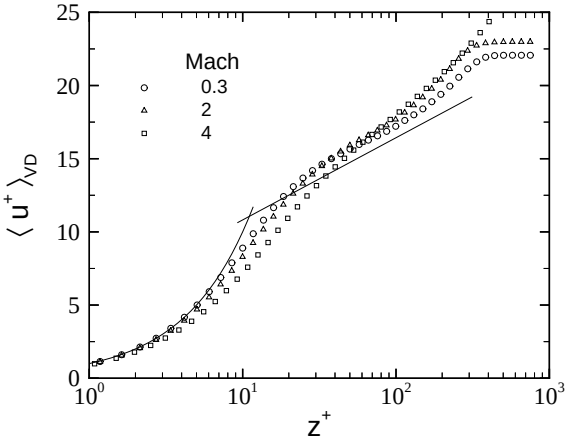

FIGURE 7. Mean streamwise velocity with Van Driest transformation. The solid lines represent $u^+ = z^+$ in the viscous sublayer, and $2.44 \log z^+ + 5.2$ in the logarithmic region.

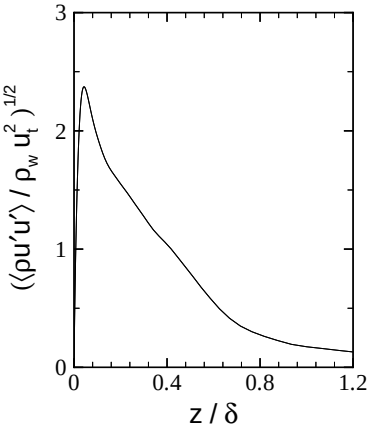

FIGURE 8. Nondimensional longitudinal turbulent intensity for the boundary layer at M=4 as it appears on Dussauge and Gaviglio[16] Fig. 4.

ever, the increased velocity slightly affects Re_θ. After the transformation, $Re_\theta = 4490$.

We use species S1 and S2 with the same molecular weight, O_2, so that the gas constant does not change when we initialize the chemistry. In this way, we avoid the introduction of aphysical pressure waves in the computational domain. We initialize the species concentrations to equilibrium values at the given mean temperature and density. The chemical composition in typical hypersonic boundary layers is not in equilibrium. However, we chose chemical equilibrium conditions to isolate the effect of turbulent fluctuations in the chemistry turbulence interaction.

The conditions chosen are representative of the boundary layer on a 26° wedge in a Mach 20 flow at an altitude of 20 km.

The initial turbulent field is in a statistically stationary state when the chemistry is not active. Thus, to study the turbulence-chemistry interaction we perform a DNS and monitor the evolution of the turbulent quantities as they depart from their original state.

Figure 9 plots the evolution of product (S2) mass-fraction, $\langle \rho_{S2} \rangle / \langle \rho \rangle$, given in large eddy turn over time periods, $\tau_\Lambda = \delta / U$. The maximum $\langle \rho_{S2} \rangle / \langle \rho \rangle$ occurs at $z = 0.07\delta$ which corresponds to the location of maximum temperature. We observe no temporal change in the chemical product formation. This is a consequence of initializing the chemistry to equilibrium. Since the average temperature does not change, neither does $\langle \rho_{S2} \rangle / \langle \rho \rangle$.

Figure 10a plots the evolution of the RMS S2 mass-fraction fluctuation, $(\rho'_{S2})_{RMS} / \langle \rho \rangle$. The magnitude of S2 fluctuations decreases in time for all locations across the layer. Figure 10b plots the magnitude of the temperature fluctuations, $T'_{RMS} / \langle T \rangle$. The initial maximum value is nearly 15% of $\langle T \rangle$. However, it decays rapidly to about 5% of $\langle T \rangle$.

Figure 11a plots the streamwise Reynolds stress, $\langle \rho u' u' \rangle / \rho_w u_\tau^2$, which is virtually unaffected by the chemical reactions. Figure 11b plots the spanwise Reynolds stress, $\langle \rho v' v' \rangle / \rho_w u_\tau^2$, and we observe that it increases in time and develops a plateau for $0.2 < \delta < 0.4$. Figure 11c plots the wall-normal Reynolds stress, $\langle \rho w' w' \rangle / \rho_w u_\tau^2$. We observe the same behavior as for the spanwise Reynolds stress. Figure 11d plots the shear Reynolds stress, $\langle \rho u' w' \rangle / \rho_w u_\tau^2$, which increases in time. Thus, all of the turbulent stresses except the streamwise Reynolds stress are increased by the chemical reactions.

Figure 12 plots the evolution of the pressure-dilatation, $\langle p' d' \rangle$. The pressure-dilatation increases initially across the layer and then decays. The magnitude is one order higher than it is when the chemistry is not active.

Conclusions

We perform direct numerical simulations of supersonic non-reacting and reacting turbulent boundary layers. The simulations are performed using a new parallel time-accurate implicit method with a low-dissipation essentially non-oscillatory (ENO) differencing method. The grid is $384 \times 256 \times 128$. The non-reacting Mach 4 turbulent simulation is in agreement with the data compilation of Dussauge and Gaviglio.[16] The endothermic chemical reaction that we consider damps the temperature fluctuations and increases the turbulent stresses, with the exception of the stream-

wise Reynolds stress. The pressure-dilatation is also increased significantly. The reduction in the temperature fluctations is consistent with our previous results concerning the decay of reacting isotropic turbulence. The increase in the Reynolds stresses may be due to the interaction between the chemical reactions and the anisotropic boundary layer.

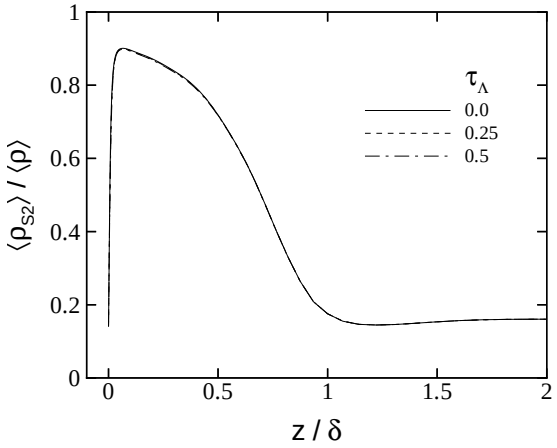

FIGURE 9. Evolution of species S2 mass-fraction for the reacting $M = 4$ simulation. Where $\tau_\Lambda = \delta/U$.

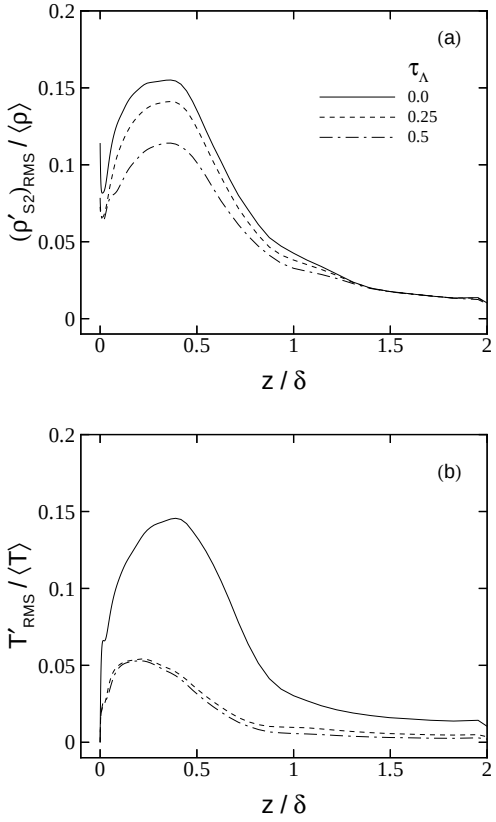

FIGURE 10. Evolution of (a) RMS S2 mass-fraction and (b) nondimensional temperature fluctuation magnitude for the reacting $M = 4$ simulation.

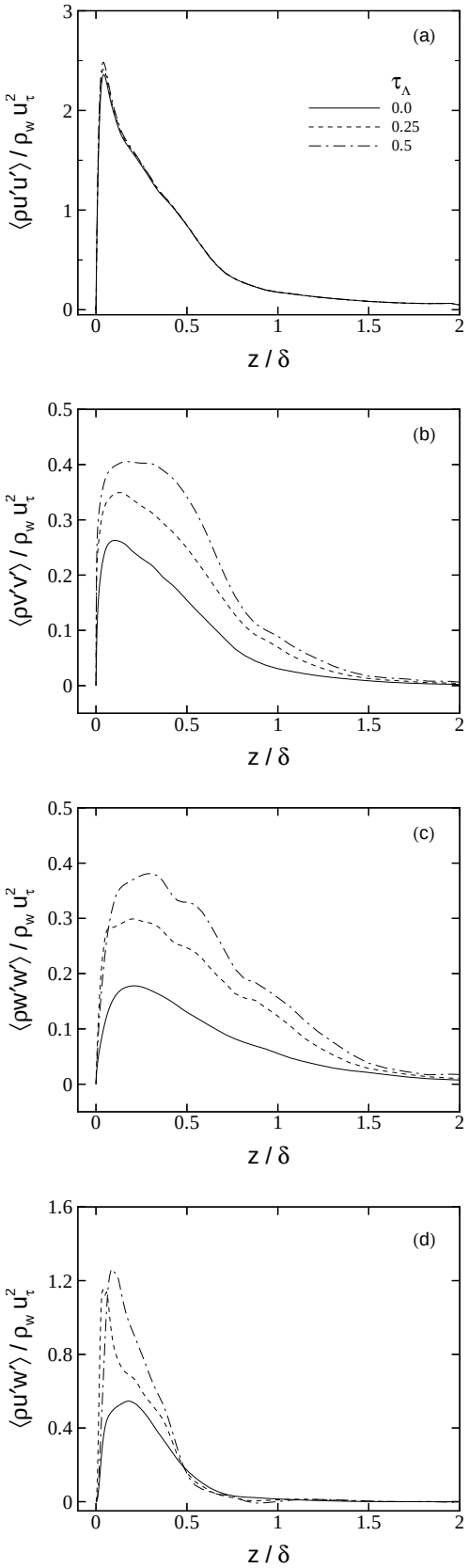

FIGURE 11. Evolution of nondimensional (a) streamwise, (b) spanwise, (c) wall-normal, and (d) shear Reynolds stresses for the reacting $M = 4$ simulation.

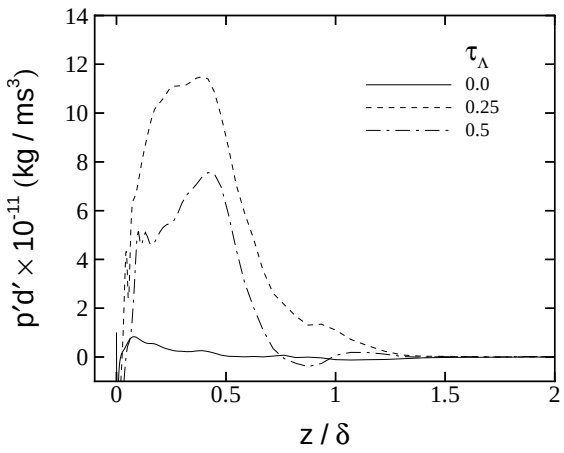

FIGURE 12. Dimensional pressure-dilatation for the reacting $M = 4$ simulation.

Acknowledgments

We would like to acknowledge support from the Air Force Office of Scientific Research Grant AF/F49620-98-1-0035. This work was also sponsored in part by the Army High Performance Computing Research Center under the auspices of the Department of the Army, Army Research Laboratory cooperative agreement number DAAH04-95-2-0003 / contract number DAAH04-95-C-0008. We would also like to thank Krishnendu Sinha for providing the mean turbulent profiles for the supersonic cases.

References

[1] Lee, J.H., "Basic governing equations for the flight regimes of aeroassisted orbital transfer vehicles," *Thermal Design of Aeroassisted orbital transfer vehicles*, ed. H.F. Nelson, *AIAA Progress in Aeronautics and Astronautics*, **96**, 3–53 (1985).

[2] Johnson, J.A., 3rd., I. Lin, and J.P. Santiago, "Turbulent collisional ionizing shock waves in argon," *J. Phys. D: Appl. Phys.*, **23** 662–72, 1990.

[3] Johnson, H., T. Seipp, and G.V. Candler, "Numerical study of hypersonic reacting boundary layer transition to cones," *AIAA Paper No. 97-2567*, 1997.

[4] M.P. Martín and G.V. Candler, "Effect of chemical reactions on decaying isotropic turbulence," To appear in Phys. Fluids, July (1998).

[5] Olejniczak, D.J., and G.V. Candler, "A Data-Parallel LU relaxation method for DNS of compressible flows," *1st International Conference in* DNS *and* LES, Louisiana, August 1997.

[6] Wright, M.J., and G.V. Candler, "A Data-Parallel LU relaxation method for reacting viscous flows," *Proceedings of Parallel CFD'95*, Elsevier Science Publishers B.V., The Netherlands, 1995.

[7] Weirs, V.G., and G.V. Candler, "Optimization of weighted ENO schemes for DNS of compressible turbulence," *AIAA Paper No. 97-1940,* July 1997.

[8] Weirs, V.G., D.J. Olejniczak, and G.V. Candler, "An implicit essentially nonoscillatory method for the direct simulation of supersonic turbulent boundary layers," *AIAA Paper No. 98-0129,*, January 1998.

[9] Gupta, R.N., J.M., Yos, R.A., Thompson, and K. Lee, "A review of reaction rates and thermodynamic and transport properties for an 11-species air model for chemical and thermal non-equilibrium calculations to 30,000 K," NASA Reference Publication 1232 (1990).

[10] Candler, G.V., W.J. Wright, and J.D. McDonald, "Data-Parallel Lower-Upper Relaxation method for reacting flows," *AIAA Journal,* 32, pp. 2380-2386, 1994.

[11] Piomelli, U., Associate Professor, Department of Mechanical Engineering, University of Maryland. Private communication.

[12] Spalart, P.R., "Direct simulation of a turbulent boundary layer up to $Re_\theta = 1410$," *Journal of Fluid Mechanics,* 187, pp. 61-98, 1988.

[13] Smits, A.J., J.P. Dussauge, "Turbulent shear layers in supersonic flow," *American Institute of Physics Press*, Woodbury, New York, 1996.

[14] Jones, W.P., and Launder, B.E.,"The prediction of laminarization with a two-equation model of Turbulence," *International Journal of Heat and Mass Transfer,* 15, pp. 301-314, 1972.

[15] Morkovin, M.V., "Effects of compressibility on turbulent flows," Favre, A.J. (ed) of *Mèchanique de la Turbulence*, pp. 367-380, CNRS.

[16] Dussauge, J.P. and Gaviglio, J., "The rapid expansion of a supersonic turbulent flow: role of bulk dilatation," *Journal of Fluid Mechanics,* 174, pp. 81-112, 1987.